INFLUENCE OF URBAN PATTERNS ON FLOODING

MARTIN BRUWIER[1], AHMED MUSTAFA[2,], DANIEL G. ALIAGA[3], SÉBASTIEN ERPICUM[4], PIERRE ARCHAMBEAU[5], GEN NISHIDA[6], XIAO WEI ZHANG[7], MICHEL PIROTTON[8], JACQUES TELLER[9] & BENJAMIN DEWALS[10]

[1,4,5,8,10]Hydraulics in Environmental and Civil Engineering (HECE), University of Liege (ULG), Belgium
martinbruwier@ulg.ac.be
[2,9] Local Environment Management and Analysis (LEMA), University of Liege (ULG), Belgium
[2,3,6,7] Computer Science Department, Purdue University, USA

ABSTRACT

The goal of this paper is to identify the respective influence of different characteristics of urban patterns on urban flooding. A set of 2,290 alternate urban patterns is generated randomly using an urban generator tool providing the geometry of buildings and their relative location to the ground, over a square area of 1 km². Steady 2-D hydraulic computations are performed for these 2,290 different urban patterns with identical hydraulic boundary conditions. The computational time is reduced by using ananisotropic porosity model. This model uses relatively coarse computational cells; but preserves information from the detailed topographic data through the use of porosity parameters. Based on the computed maps of water depths for the 2,290 urban patterns, a sensitivity analysis based on a multiple linear regression is performed to outline the most influential urban characteristics.

Keywords: Urbanization; porosity model; urban inundation modeling; urban planning.

1   INTRODUCTION

The geometric characteristics of urban patterns (e.g. street width, orientation or curvature) have a strong influence on flow properties during urban flooding. They influence the discharge partition between the streets as well as the flow depths and velocities, both within the considered urban area as well as upstream and downstream. In this paper, a systematic analysis is performed to determine the influence of various characteristic of urban patterns on urban flooding.

The study considers 10 parameters controlling the urban pattern: average street length, street orientation, street curvature, major and secondary street widths, parks coverage, maximum parcel area and three different building's setbacks. By varying the values of the different urban parameters, a set of 2,290 synthetic urban networks are generated.

The high number of urban networks generated by the urban generator tool makes the computation challenging using classical hydraulic models. Subgrid models enable improvements of the computational efficiency by enabling a coarsening of the computational grid, while preserving the essence of the detailed topographic information available at a fine scale. Anisotropic porosity models are one kind of subgrid models for which fine scale information are maintained at the coarse scale by including porosity parameters in the governing equations (Sanders et al., 2008). Storage porosities reproduce the available storage volume within the cells and conveyance porosities consider the effects of buildings on the fluxes evaluated along the edges. An additional drag loss term is used to consider the resistance of obstacles to the flow. This allows an increase of the grid spacing by roughly one order of magnitude, while preserving a similar level of accuracy as with a fine mesh (Schubert and Sanders, 2012; Kim et al., 2014; Kim et al., 2015).

In this paper, the relationship between characteristics of urban patterns and flooding is explored through a multiple linear regression. The results of the sensitivity analysis are exemplified by comparing the inundation water depths resulting from different combinations of urban characteristics.

The findings of this study contribute to a better understanding of the interactions between complex urban systems and flooding to guide more flood-proof urban developments.

2   METHOD

This study followed the methodology presented in Figure 1 for which three different tools had been developed:

- An urban generator tool generated 2,290 synthetic urban networks over a 1 km^2 area through the selection of the values of 10 parameters controlling the building geometries and locations (section 2.1).
- A porosity-based hydraulic model computed the flow characteristics for the 2,290 urban networks with identical hydraulic boundary conditions (section 2.2). Indicators of the flooding intensity were determined from the computed maps of water depths.

- A sensitivity analysis based on a multiple linear regression was performed to highlight the specific influence of the different urban characteristics on the inundation indicators (section 2.3.2).
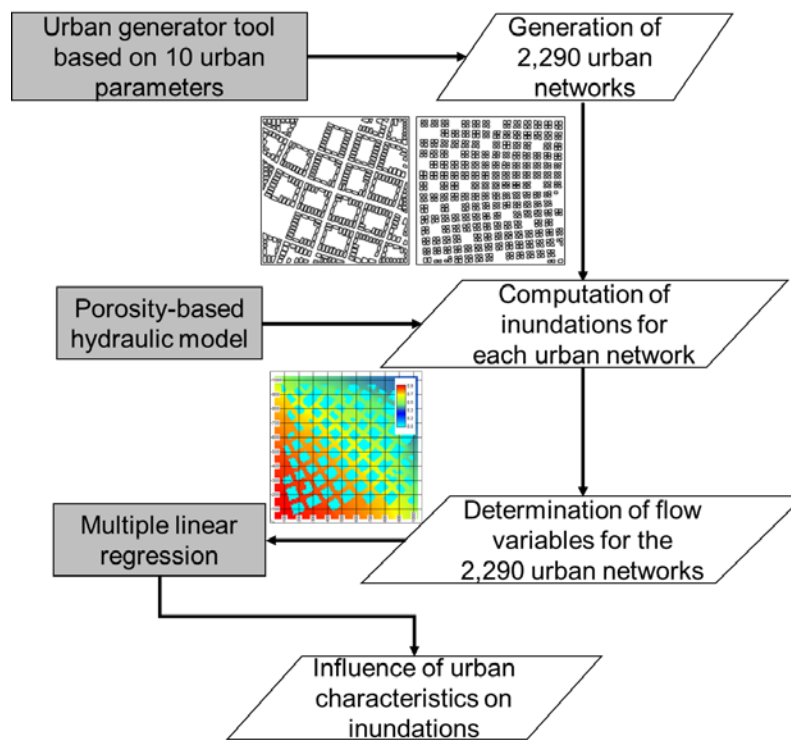
Figure 1. Methodology for the determination of the influence of urban patterns on urban flooding.
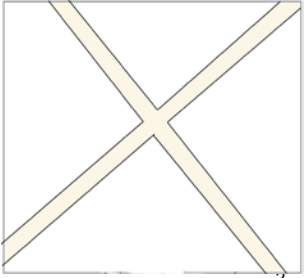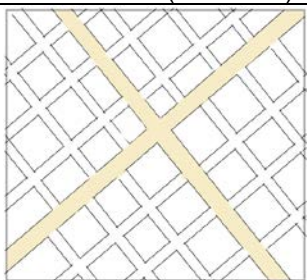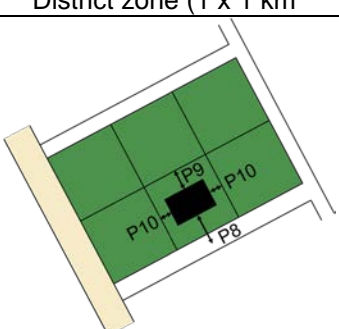
2.1 Urban generator tool

The urban generator tool is based on a procedural modeling (Parish and Müller, 2001) which automatically generates urban networks given a set of rules and parameter values (Prusinkiewicz and Lindenmayer, 1990). The outputs of the urban generator consist of locations and shapes of streets and buildings. While this approach was originally proposed by Parish and Müller (2001), the tensor field using the approach of Chen et al. (2008) was adapted in this study for street generation, as it supports more variations in the street networks. The urban generator is based on 10 input parameters (Table 1) and follows the five-step process sketched in Figure 2.

The 2,290 urban networks were generated based on input parameters selected randomly in the range between the minimum and maximum values reported in Table 1. Once the input parameters are fixed, the urban generator produces a single urban network without including any random seeds. The ranges of variation of the input parameters are representative of real-world information obtained from cadastral data for a building area of about 500 km²in Wallonia (Belgium).

Table 1. Input parameters and building coverage for the urban generator engine.

ID	Parameter	Minimum value (P_{min})	Maximum value (P_{max})
P1	Averagestreet length	40 m	400 m
P2	Street orientation	0°	180°
P3	Street curvature	0 rad.	0.42 rad.
P4	Major street width	16 m	33 m
P5	Minor street width	8 m	16 m
P6	Park coverage	5%	40%
P7	Maximum parcel area	300 m^2	1,100 m^2
P8	Building front setback	0 m	5 m
P9	Building rear setback	0 m	5 m
P10	Building side setback	0 m	5 m
BC	Building coverage	0%	42.8%

Step	Description	Input parameters	Illustration
1	Definition of grid points with a spatial resolution of 1 m		
2	Definition of the shape of two orthogonal major streets	P1 to P4	District zone (1 x 1 km^2)
3	Tracing of the local streets based on the tensor field	P1 and P5	District zone (1 x 1 km^2
4	Definition of parks and parcels	P6 and P7	District zone (1 x 1 km^2
5	Construction of buildings in the parcels	P8 to P10	Parcel zone

Figure 2. Flow chart of the urban generator tool.

2.2 Flow computations

2.2.1 Hydraulic conditions

The 2,290 urban networks were placed over a slopeless urban zone of 1 x 1 km^2, where buildings were considered sufficiently high for not being overtopped by the flooding. The left and bottom sides of the urban zones were the upstream sides, while the right and top sides were the downstream ones. At the upstream sides, a steady discharge of 200 m^3/s and uniformly distributed was prescribed as a boundary condition. At the downstream sides, free flow conditions were assumed. The Manning roughness coefficient of the bottom was n = 0.04 sm$^{-1/3}$ over the entire domain. Flow characteristics were computed on a Cartesian grid of 10 m x 10 m.

2.2.2 Anisotropic porosity model

Hydraulic computations were performed with the hydraulic model WOLF 2-D, which has been extensively used for studies of inundations in urban areas (Ernst et al., 2010; Beckers et al., 2013; Bruwier et al., 2015; Detrembleur et al., 2015). WOLF 2-D solves the fully two-dimensional shallow-water equations on Cartesian grids based on a conservative finite volume scheme with a flux vector splitting technique (Erpicum et al., 2010). An anisotropic porosity model has been included in the existing WOLF 2-D which has been validated over multiple test cases (e.g. Arrault et al., 2016).

The integral form of the governing equations of anisotropic porosity models (Sanders et al., 2008) is discretized with a finite volume scheme for a cell j and its K edges k as in Eq. [1].

$$\frac{\partial \langle \mathbf{U} \rangle_j}{\partial t} + \frac{1}{\Omega_j} \sum_{k=1}^{K} [\mathbf{F}]_k \, \partial \Omega_k = \langle \mathbf{S} \rangle_j \qquad [1]$$

where,

$$\langle \mathbf{U} \rangle = \phi \begin{bmatrix} \langle h \rangle \\ \langle uh \rangle \\ \langle vh \rangle \end{bmatrix},$$

$$[\mathbf{F}] = \psi \begin{bmatrix} [uh] & [vh] \\ [u^2 h] + \frac{g}{2}\left([h]^2 - h_{\eta_0,x}^2\right) & [uvh] \\ [uvh] & [v^2 h] + \frac{g}{2}\left([h]^2 - h_{\eta_0,y}^2\right) \end{bmatrix}, \qquad [2]$$

$$\langle \mathbf{S} \rangle = -\phi \begin{bmatrix} 0 \\ \left(c_D^f + c_{D,x}^b\right)\langle uV \rangle \\ \left(c_D^f + c_{D,y}^b\right)\langle vV \rangle \end{bmatrix}.$$

where t is the time, Ω the total area of the cell, $\partial \Omega$ the total length of the edge, h the water depth, u and v the x- and y- velocity components, $V = \sqrt{u^2 + v^2}$, g the gravitational acceleration, c_D^f the roughness coefficient and c_D^b the drag coefficient estimated consistently with the simplified method proposed by Schubert et al. (2012). The term $h_{\eta_0}^2$ corresponds to the water depth computed for a piecewise stationary water level η_0. The notations $\langle \ \rangle_j$ and $[\ ]_k$ refer respectively to flow variables at the cells and for their reconstruction to the edges.

The divergence formulation of the bed slope (Valiani and Begnudelli, 2006) term is used in Eq. [2] in which the stationary water level η_0 of a cell is determined as a linear combination of the water levels at its edges minimizing the error in the energy balance (Bruwier et al., 2016).

The storage porosity ϕ_j and the conveyance porosity ψ_k are respectively defined by Eq. [3] and [4]:

$$\phi_j = \frac{\Omega_{f,j}}{\Omega_j}, \qquad [3]$$

$$\psi_k = \frac{\partial \Omega_{f,k}}{\partial \Omega_k}. \qquad [4]$$

where $\Omega_{f,j}$ and $\partial \Omega_{f,k}$ represent respectively the cell area and the edge length, available for water.

The stability condition of the scheme is given in Eq. [5] considering the porosity parameters (Sanders et al., 2008). The criterion writes, with $c = V + \sqrt{gh}$ the wave celerity:

$$\Delta t \leq CFL \min\left(\frac{1}{c} \frac{\phi \Omega}{\max(\psi \, \partial \Omega)}\right), \qquad [5]$$

Since low storage porosities can reduce dramatically the computational time, cells with a storage porosity lower than a threshold $\phi_{\min}$ are removed from the computation domain.

Based on a comparison between results computed at the coarse scale with the anisotropic porosity model using a drag coefficient of $c_D^b = 3$ and a threshold porosity $\phi_{\min} = 0.1$ and results computed at the fine scale, for three arbitrary urban networks, average errors on water depths at the upstream sides are estimated around few millimeters (<1 cm).

2.3 Determination of the influence of urban characteristics on inundation characteristics

In this paper, the intensity of a flooding was assessed through inundation indicators computed as quantiles of computed water depths $h_{Q\%}$ either over the whole inundated area or along the upstream sides of the domain. The influence of 11 characteristics of urban patterns was evaluated on these inundation indicators: the 10 urban parameters (P1 to P10) used as inputs for the urban generator tool and the building coverage (BC) representing the part of building areas over the total urban zone.

Using x_i with $i = 1, ..., 11$ and y to represent respectively the 11 urban characteristics and the inundation indicator, two non-dimensional forms of the variables x_i and y are defined: a normalized form and a standardized form.

The normalization forms of the variables $\check{x}_i$ and $\hat{y}$ are computed with Eq. (6) based on the minimum ($x_{\min}$ and $y_{\min}$) and maximum ($x_{\max}$ and $y_{\max}$) values over the 2,290 computed urban networks:

$$\check{x}_i = \frac{x_i - x_{i,\min}}{\left(x_{i,\max} - x_{i,\min} \right)} \quad \text{and} \quad \hat{y} = \frac{y - y_{\min}}{\left(y_{\max} - y_{\min} \right)}, \tag{6}$$

This normalization enables comparing the relative variations of variables within their own ranges of values.

The standardized forms of the variables $\bar{x}_i$ and $\bar{y}$ are rewritten based on the mean ($x_{i,\mathrm{mean}}$ and y_{mean}) and standard deviation ($x_{i,\mathrm{std}}$ and y_{std}) values over the 2,290 computed urban networks:

$$\bar{x}_i = \frac{x_i - x_{i,\mathrm{mean}}}{x_{i,\mathrm{std}}} \quad \text{and} \quad \bar{y} = \frac{y - y_{\mathrm{mean}}}{y_{\mathrm{std}}}, \tag{7}$$

The standardization is used for the multiple linear regression presented hereafter.

The matrix notations $\mathbf{X}$ and $\mathbf{Y}$ are defined with $\bar{x}_1^n$ and $\bar{y}^n$ the values of $\bar{x}_i$ and $\bar{y}$ corresponding to the nth computed urban network:

$$\mathbf{X} = \begin{bmatrix} \bar{x}_1^1 & \bar{x}_2^1 & \dots & \bar{x}_{11}^1 \\ \bar{x}_1^2 & \bar{x}_2^2 & \dots & \bar{x}_{11}^2 \\ \vdots & \vdots & \ddots & \vdots \\ \bar{x}_1^{2,290} & \bar{x}_2^{2,290} & \dots & \bar{x}_{11}^{2,290} \end{bmatrix} \quad \text{and} \quad \mathbf{Y} = \begin{bmatrix} \bar{y}^1 \\ \bar{y}^2 \\ \vdots \\ \bar{y}^{2,290} \end{bmatrix}. \tag{8}$$

A multiple linear regression is used to determine the least squares linear parameters $\mathbf{A} = [a_1, a_2, ..., a_{11}]^{\mathrm{T}}$ which represent the sensitivity of the inundation indicator with respect to each urban characteristic.

$$\mathbf{A} = \left(\mathbf{X}^{\mathrm{T}} \mathbf{X} \right)^{-1} \mathbf{X}^{\mathrm{T}} \mathbf{Y}. \tag{9}$$

3   RESULTS AND DISCUSSION

The sensitivity parameters a_i were computed from Eq. (8) for inundation indicators between $h_{85\%}$ and $h_{95\%}$ over all the inundated area and between $h_{50\%}$ and $h_{95\%}$ along the upstream sides of the domain, with a constant quantile step of 5%. Figure 4 compares the minimum and maximum values of the computed values of a_i depending on the domain over which quantiles values are determined. This shows that sensitivity parameters are weakly influenced by the chosen inundation indicator.
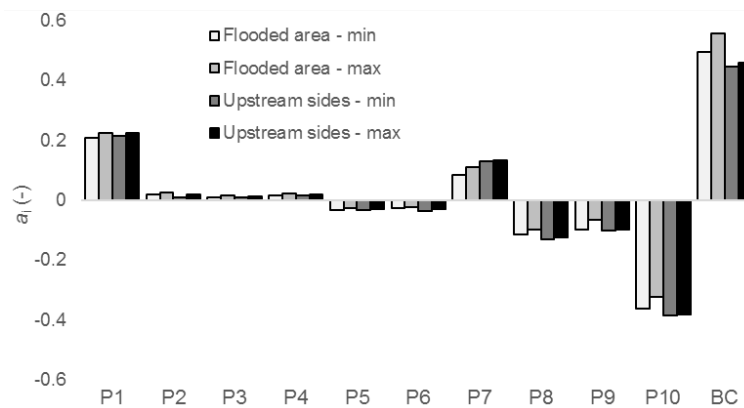
Figure 4. Minimum (- min) and maximum (- max) values of the linear parameters a_i depending on the domain over which quantiles are determined for the 11 urban characteristics.

In the following of the paper, the $h_{90\%}$ value computed along the upstream sides was used to discuss the influence of urban characteristics on inundation water depths (Table 2). The correlation coefficient associated to the multiple linear regression was equal to R = 0.92.

The building coverage (BC) was the urban characteristic having the highest influence on inundation water depths ($a_{11} = 0.457$). This strong influence suggests to fixing the building coverage to constant values in future studies to highlight more clearly the influence of other urban patterns on flooding.

The building side setback (P10), which represented the distance between two adjacent buildings, was the urban characteristic with the second highest influence on inundation characteristics ($a_{10} = -0.385$). The negative value indicates that inundation characteristics tend to be more severe if the value of P10 decreases, as a reduction of the conveyance capacity between buildings. This was exemplified by comparing the $h_{90\%}$ values for the two urban networks represented in Figures 5a and 5b, for which the main differences were the building setback parameters. The inundation water depths were well higher for the urban network with a setback side value equaled to 0 (Figure 5b). Parameter P10 had about three times as much influence as the other building setbacks (P8 and P9). Indeed, the inundation indicator in Figure 5d was lower than in Figure 5c because the distances between adjacent buildings (P10) are higher, even if the building setbacks P8 and P9 decreased.

The third highest sensitivity parameter value was related to the average street length (P1). The inundation water depths increased with a rise in this urban characteristic. Comparing the urban networks of Figure 5e and Figure 5f, large groups made of multiple buildings increased for high values of P1. Since the void area enclosed in these groups of buildings hardly contributes to the conveyance of the flow, inundation water depths increased with an augmentation of the value of P1.

Urban inundation water depths were weakly influenced by the values of the street orientation (P2) and street curvature (P3), which did not affect the conveyance ability of the urban network. The validity of this funding should be tested for more dynamic flow conditions (i.e. higher flow velocity). Here the maximum value of the Froude number in the urban area did not exceed 0.4. More surprising were the low sensitivity parameters values obtained for streets widths (P4 and P5) and park coverage (P6). This is certainly related to the absence of constraints on the value of the building coverage in the urban generator tool, leading to a mix of the effects of parameters P4 to P6 with the high influence of the building coverage value (BC). Therefore, the building coverage will be set to constant values in future analysis.

Table 2. Sensitivity parameters computed for $h_{90\%}$ along the upstream sides with $a_{max} = a_{11}$.

	P1	P2	P3	P4	P5	P6	P7	P8	P9	P10	BC
a_i	0.127	0.010	0.011	0.018	-0.032	-0.031	0.133	-0.125	-0.102	-0.385	0.457
$\dfrac{a_i}{a_{max}}$	47%	2%	3%	4%	-7%	-7%	29%	-27%	-22%	-84%	100%
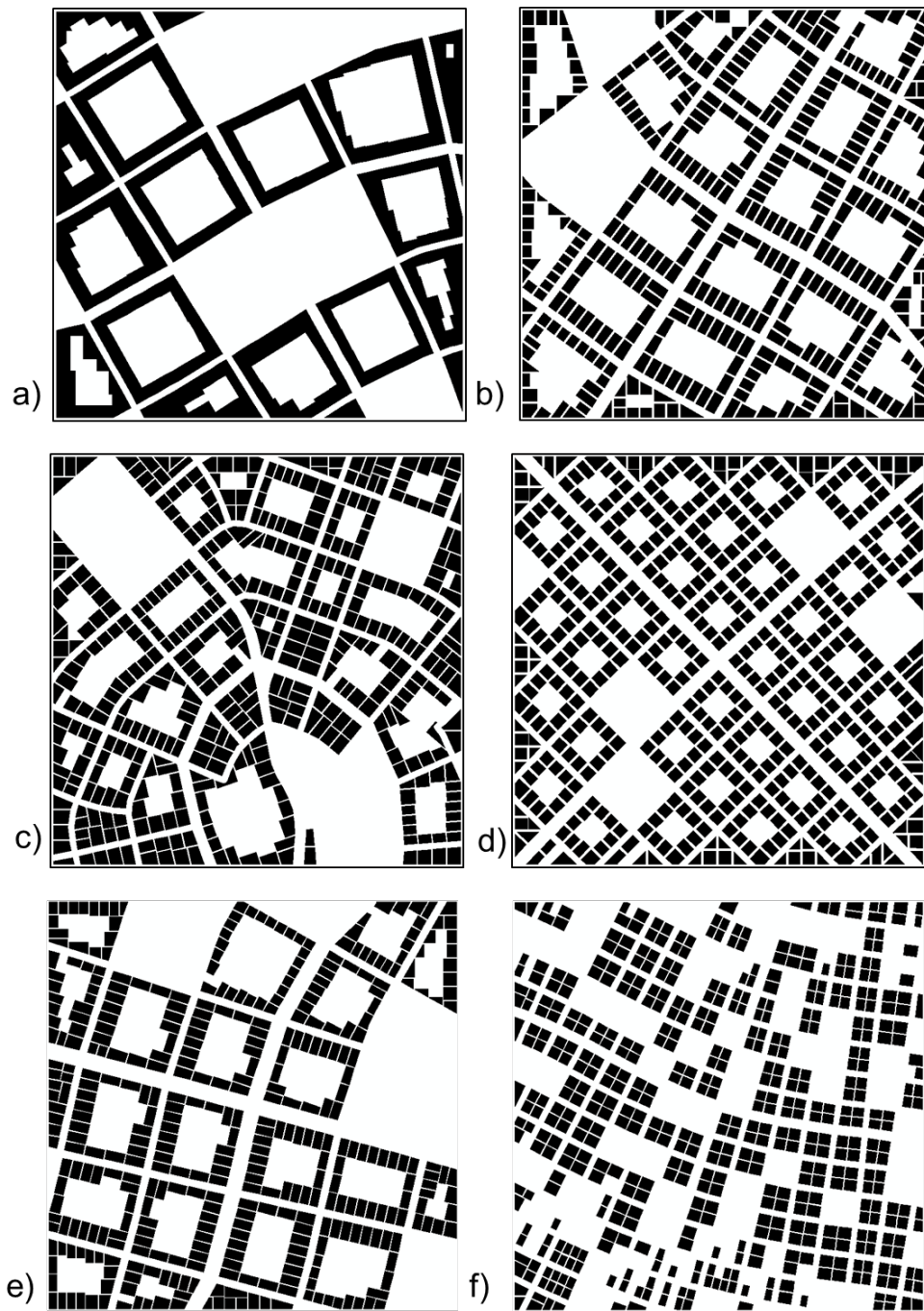
	P1	P2	P3	P4	P5	P6	P7	P8	P9	P10	BC	$h_{90\%}$
a)	0.57	0.28	0.63	0.38	0.58	0.65	0.74	**0.00**	**0.00**	**0.00**	0.74	0.73
b)	0.50	0.95	0.72	0.47	0.55	0.14	0.86	**0.32**	**0.57**	**0.64**	0.75	0.33
c)	0.32	0.09	0.93	0.23	0.10	0.14	1.00	**0.36**	**0.39**	**0.46**	0.88	0.49
d)	0.29	0.24	0.02	0.59	0.23	0.10	0.90	**0.22**	**0.25**	**0.71**	0.89	0.37
e)	**0.48**	0.52	0.55	0.85	0.38	0.57	0.75	0.48	0.34	0.41	0.71	0.45
f)	**0.09**	0.90	0.10	0.19	0.25	0.66	0.49	0.26	0.61	0.44	0.71	0.28

Figure 5. Normalized values of the urban characteristics $\hat{x}_i$ and inundation indicator $\hat{y}$ for different computed urban networks.

Over the 2,290 computed urban networks, the three urban configurations leading to the highest flow depths are represented in Figure 6. These urban networks correspond to building setbacks equal to 0 for which enclosed areas free for water are surrounded by buildings, limiting hence the available space to convey the flow. The urban network with the highest inundation indicator (Figure 6a) was characterized by a very high average street length (P1 = 1.00), as for Figure 6c (P1 = 0.81). The second highest inundation indicator was computed for an urban network combining high values of average street length P1, average parcel areas P7 and building coverage BC.

	P1	P2	P3	P4	P5	P6	P7	P8	P9	P10	BC	$h_{90\%}$
a)	1.00	0.36	0.64	0.42	0.19	0.37	0.51	0.00	0.00	0.00	0.63	1.00
b)	0.68	0.55	0.33	0.14	0.14	0.12	0.78	0.00	0.00	0.00	0.92	1.00
c)	0.81	0.30	0.28	0.54	0.16	0.46	0.51	0.00	0.00	0.00	0.67	0.98
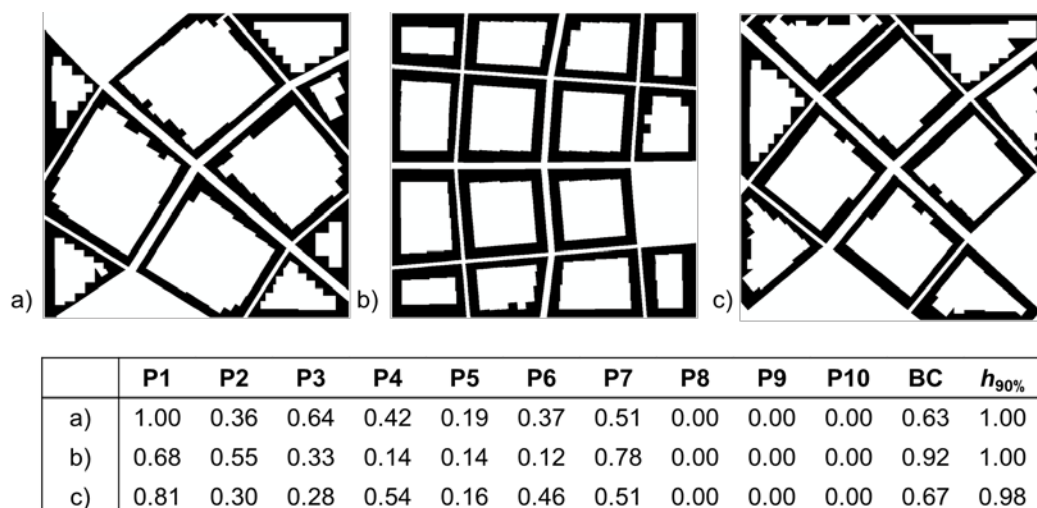
Figure 6. Normalized values of the urban characteristics $\hat{x}_i$ and inundation indicator $\hat{y}$ for the three urban networks leading to the highest values of the inundation indicator.

4   CONCLUSIONS

The aim of this paper is to present a methodology to evaluate the sensitivity of urban flooding to different urban characteristics. By varying the values of 10 urban pattern parameters, 2,290 urban networks are generated by an urban generator model. Using identical hydraulic conditions, inundations characteristics are computed for each urban network with a shallow-water model with porosity which enables to reduce the computational cost by using a coarse grid, while preserving the detailed topographic data to some extent through porosity parameters. A sensitivity analysis is performed based on a multiple linear regression to highlight the influence of several urban characteristics on the urban inundation water depths.

The preliminary results show that the building coverage is the urban characteristic with the highest influence on inundation water depths. This strong influence suggests to fixing the building coverage to a constant value in future studies to highlight more clearly the influence of other urban patterns on flooding. Additionally, the values of the sensitivity parameters suggest that average street length and building side setback have a higher impact on inundation water depths than other urban characteristics.

REFERENCES
Arrault, A., Finaud-Guyot, P., Archambeau, P., Bruwier, M., Erpicum, S., Pirotton, M. & Dewals, B. (2016). Hydrodynamics of Long-Duration Urban Floods: Experiments and Numerical Modelling. *Natural Hazards and Earth System Sciences,* 16, 1413–1429.
Beckers, A., Dewals, B., Erpicum, S., Dujardin, S., Detrembleur, S., Teller, J., Pirotton, M. & Archambeau, P. (2013). Contribution of Land Use Changes to Future Flood Damage along the River Meuse in the Walloon Region. *Natural Hazards and Earth System Sciences,* 13, 2301–2318.
Bruwier, M., Archambeau, P., Erpicum, S., Pirotton, M. & Dewals, B. (2016). *Discretization of the Divergence Formulation of the Bed Slope Term in the Shallow-Water Equations and Consequences in Terms of Energy Balance.* Applied Mathematical Modelling, 40, 7532–7544.
Bruwier, M., Erpicum, S., Pirotton, M., Archambeau, P. & Dewals, B.J. (2015). Assessing the Operation Rules of a Reservoir System based on a Detailed Modelling Chain. *Natural Hazards and Earth System Sciences* 15, 365–379.
Chen, G., Esch, G., Wonka, P., Müller, P. & Zhang, E. (2008). Interactive Procedural Street Modeling. *ACM Transactions on Graphics,* 27(3), Article 103, 1-10.

Detrembleur, S., Stilmant, F., Dewals, B., Erpicum, S., Archambeau, P. & Pirotton, M. (2015). Impacts of Climate Change on Future Flood Damage on the River Meuse, with a Distributed Uncertainty Analysis. *Natural Hazards,* 77, 1533–1549.

Ernst, J., Dewals, B.J., Detrembleur, S., Archambeau, P., Erpicum, S. & Pirotton, M. (2010). Micro-Scale Flood Risk Analysis based on detailed 2D Hydraulic Modelling and High Resolution Geographic Data. *Natural Hazards,* 55, 181–209.

Erpicum, S., Dewals, B.J., Archambeau, P. & Pirotton, M. (2010). Dam Break Flow Computation based on an Efficient Flux Vector Splitting. *Journal of Computational and Applied Mathematics,* 234, 2143–2151.

Kim, B., Sanders, B.F., Famiglietti, J.S. & Guinot, V. (2015). Urban Flood Modeling with Porous Shallow-Water Equations: A case Study of Model Errors in the Presence of Anisotropic Porosity. *Journal of Hydrology,* 523, 680–692.

Kim, B., Sanders, B.F., Schubert, J.E. & Famiglietti, J.S. (2014). *Mesh Type Tradeoffs in 2D Hydrodynamic Modeling of Flooding with a Godunov-based Flow Solver.* Advances in Water Resources, 68, 42–61.

Parish, Y.I.H. & Müller, P. (2001). Procedural Modeling of Cities. *Proceedings of the 28th Annual Conference on Computer Graphics and Interactive Techniques, SIGGRAPH '01.*

Prusinkiewicz, P. & Lindenmayer, A. (1990). *Modeling of Cellular Layers. The Algorithmic Beauty of Plants.* Springer, 145–174.

Sanders, B.F., Schubert, J.E. & Gallegos, H.A. (2008). Integral Formulation of Shallow-Water Equations with Anisotropic Porosity for Urban Flood Modeling. *Journal of Hydrology,* 362, 19–38.

Schubert, J.E. & Sanders, B.F. (2012). *Building Treatments for Urban Flood Inundation Models and Implications for Predictive Skill and Modeling Efficiency.* Advances in Water Resources, 41, 49–64.

Valiani, A. & Begnudelli, L. (2006). Divergence Form for Bed Slope Source Term in Shallow Water Equations. *Journal of Hydraulic Engineering,* 132, 652–665.